Generation of tunable, 100–800 MeV quasi-monoenergetic electron beams from a laser-wakefield accelerator in the blowout regimea)

S. Banerjee, N. D. Powers, V. Ramanathan, I. Ghebregziabher, K. J. Brown, C. M. Maharjan, S. Chen, A. Beck, E. Lefebvre, S. Y. Kalmykov, B. A. Shadwick, and D. P. Umstadter

Citation: Physics of Plasmas (1994-present) **19**, 056703 (2012); doi: 10.1063/1.4718711
View online: http://dx.doi.org/10.1063/1.4718711
View Table of Contents: http://scitation.aip.org/content/aip/journal/pop/19/5?ver=pdfcov
Published by the AIP Publishing

Generation of tunable, 100–800 MeV quasi-monoenergetic electron beams from a laser-wakefield accelerator in the blowout regime[a)]

S. Banerjee,[1,b)] N. D. Powers,[1] V. Ramanathan,[1] I. Ghebregziabher,[1] K. J. Brown,[1] C. M. Maharjan,[1] S. Chen,[1] A. Beck,[2] E. Lefebvre,[2] S. Y. Kalmykov,[2] B. A. Shadwick,[2] and D. P. Umstadter[1]
[1]*Department of Physics and Astronomy, University of Nebraska, Lincoln, Nebraska 68588-0299, USA*
[2]*CEA, DAM, DIF, 91297 Arpajon Cedex, France*

(Received 4 January 2012; accepted 12 April 2012; published online 23 May 2012)

In this paper, we present results on a scalable high-energy electron source based on laser wakefield acceleration. The electron accelerator using 30–80 TW, 30 fs laser pulses, operates in the blowout regime, and produces high-quality, quasi-monoenergetic electron beams in the range 100–800 MeV. These beams have angular divergence of 1–4 mrad, and 5%–25% energy spread, with a resulting brightness 10^{11} electrons mm^{-2} MeV^{-1} $mrad^{-2}$. The beam parameters can be tuned by varying the laser and plasma conditions. The use of a high-quality laser pulse and appropriate target conditions enables optimization of beam quality, concentrating a significant fraction of the accelerated charge into the quasi-monoenergetic component. © *2012 American Institute of Physics*. [http://dx.doi.org/10.1063/1.4718711]

I. INTRODUCTION

The development of high-power, short pulse lasers has led to the development of quasi-monoenergetic electron accelerators based on the process of laser wakefield acceleration[1–10] and approaches the GeV energy range.[11–18] Experiments show that these electron beams are produced in a unique plasma structure—an electron density "bubble"[19–22]—trailing a relativistically intense laser pulse.[23–28] The bubble forms behind the driver, when the laser ponderomotive force creates complete electron cavitation (due to their high inertia, fully stripped ions remain immobile). Nonlinear evolution of the driver causes variations in the bubble shape, which triggers injection of ambient plasma electrons resulting in the formation of a collimated, high-energy, quasi-monoenergetic electron beam.[29–33]

In order to better understand and control the process of wakefield acceleration and obtain high-brightness, high-energy electron beams with low longitudinal and transverse emittance, it is necessary to consider in detail the process of wakefield acceleration. As is well known on the basis of extensive theoretical and experimental work over the past two decades, when a high-power laser pulse propagates through an underdense medium, strong longitudinal forces come into play.[34] These arise from the fact that the ponderomotive force of the laser expels electrons along the propagation axis. The ions, however, are relatively immobile and the resulting field distribution corresponds to an electron plasma wave moving at a speed governed by the density of the medium, which in the underdense regime is close to the speed of light. Energetic electrons are produced when the free electrons in the plasma are trapped and accelerated by the wave. As has been known for a long time, the ideal situation for generating the most stable and highest amplitude wakes is to have the plasma resonant with the laser. Previous experiments with long pulse lasers achieved resonance by self-modulation of the pulse. However, this led to a large number of accelerating structures leading to an electron beam with a large energy spread. While the resonance condition could have been satisfied in the long pulse regime by using a low enough density, this was not useful since the maximum electric field is proportional to n_e, and a minimum density is required in order to have a large enough field to produce relativistic electrons. With the availability of short pulse lasers, it is now possible to meet the resonance conditions at much higher density and produce high-energy quasi-monoenergetic distribution.

In the strongly nonlinear regime, the matching conditions deviate significantly from that obtained using simple linear theory. This regime is characterized by the fact that the laser power P_L is much higher than the critical power $P_c = 16.8 n_c/n_p$ GW, where n_c is the critical density and n_p is the plasma density. Under these conditions, a cavitated region is created behind the laser pulse. The resulting electrostatic force causes plasma oscillations to be setup resulting in the formation of a wakefield. Starting with the early work of Pukhov and Meyer-ter-Vehn,[25] it has been demonstrated that electrons can be injected into this wake, and produce a quasi-monoenergetic electron beam at the exit of the plasma. The phenomenological work of Lu *et al.*[28] provided a prescription for optimal wakefield acceleration in the regime $a_0 > 2$.

In this paper, we report a detailed parametric study of wakefield acceleration in this strongly nonlinear (blowout regime). We study the process of generation of high-energy quasi-monoenergetic beams in a broad range of laser and plasma parameters. A prescription is provided to optimize the beam characteristics so as to produce high-quality

[a)]Paper UI2 6, Bull. Am. Phys. Soc. **56**, 323 (2011).
[b)]Invited speaker. Author to whom correspondence should be addressed. Electronic mail: sudeep@unl.edu.

quasi-monoenergetic bunches.[44–47] The process is tunable and scalable to high-energies and provides a prescription for the generation of high-brightness electron beams by a laser wakefield accelerator.[36–38]

II. EXPERIMENTAL SETUP

The experiments were carried out with the 100 TW diocles laser system. The system produces linearly polarized pulses with a central wavelength 0.805 μm. The maximum energy is 3.5 J at 10-Hz repetition rate and pulse full width at half-maximum (FWHM) $\tau_L = 30$ fs. The laser beam is incident on a deformable mirror that operates in a feedback loop with a wavefront sensor. The 70-mm diameter laser pulse with spatial aberrations corrected, is focused to a nearly diffraction limited spot (Strehl ratio 0.95) using a one meter focal length dielectric-coated off-axis paraboloid. The intensity profile in the central spot (shown in the inset of Fig. 1) allows a Gaussian fit with a radius $r_0 = 13.6\,\mu$m. High-energy beams were generated using 30–90 TW laser power on target. The laser pulse was spatially and temporally characterized at full power using a multi-stage beam sampling system. The energy on target was varied using a combination of a waveplate and polarizers. The temporal duration is optimized by varying the separation between the compressor gratings, and adjusting the second and third order phase by use of a spectral phase modulator (dazzler). The shot-to-shot pointing stability of the laser pulse on target was $\pm 7\mu$ rad.

The experimental setup is presented in Fig. 1. The target is a high-density jet of neutral helium produced by 3 and 4 diameter cylindrical nozzles (Laval type) as well as 5 and 10 mm long slit nozzles. The neutral density profile (characterized interferometrically) has symmetric downramps along the edges extending over 0.5 mm for the cylindrical nozzles, 0.75 mm for the 5 mm slit nozzle, and 1 mm for the 10 mm slit nozzle, with a flat-top central region. The laser pulse is focused close to the front edge of the nozzle. During the experiments, an equivalent plane imaging system locates the longitudinal position of the focal plane with a precision of ± 0.5 mm. The focused pulse fully ionizes the medium producing a plasma with $n_{e0} = 0.4 - 2 \times 10^{19}\,\mathrm{cm}^{-3}$. For $n_{e0} < 10^{19}\,\mathrm{cm}^{-3}$, images of the plasma emission at 800 nm show a uniform laser-created plasma column spanning the entire jet length. The accelerated electrons exiting the plasma impinge on a fluorescent screen (LANEX) that is imaged with a 12-bit CCD.

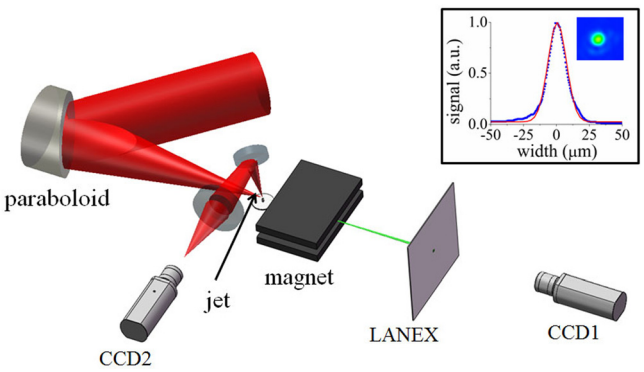

FIG. 1. Schematic of the experimental setup. The high-power laser pulse is focused using a 1-m focal length, dielectric coated, off-axis paraboloid at the front edge of a supersonic helium gas jet. The electron beam passes through a magnetic spectrometer consisting of a uniform rectangular magnetic field and a drift free region and then impinges on a LANEX screen. Optical emission from the LANEX is imaged onto the CCD1 to measure the beam angular divergence and energy spectrum, along the non-dispersive and dispersive axes respectively. The propagation of the optical pulse through the medium is monitored by imaging the Thomson-scattered light using CCD2. Inset: image of the laser focal spot in vacuum (full-power shot) and its vertical (blue/dark gray) and horizontal (red/light gray) lineouts.

The absolute response of LANEX to electrons, calibrated using an 18 MeV radio-frequency linear accelerator (Siemens Primus), is used to obtain the charge in a specified energy interval. The calibration with the low-energy electron source can be extrapolated to higher energies based on the fact that the energy deposition curve for electrons in LANEX is invariant in the range 10–1000 MeV.[39] Electron energy is measured using different magnetic spectrometers operating in a slit-free geometry and having a range of 20–800 MeV. The energy resolution is better than 10% at 500 MeV, and rapidly degrades beyond 800 MeV. The spectrometer response function has been modeled with the General Particle Tracer (GPT) code,[40–43] which propagates the electron beam from source to detector. The final energy distribution is obtained, taking into account the finite beam divergence.

III. OPTIMAL ELECTRON BEAMS FROM 3-4 mm JETS

A detailed empirical study was performed to obtain (in a reproducible way) and optimize (energy, energy spread, divergence, and stability) the electron beam produced by high-power, short laser pulses. We studied in detail the dependence of the electron beam characteristics on both laser and plasma parameters. It was empirically ascertained that production of stable, quasi-monoenergetic, high-energy beams needs the laser power above 30 TW, pulse duration 30 fs, nanosecond laser contrast 2×10^{-8}, and focal spot free of aberrations. Any deviations from these conditions led to a poor quality beam (lower energy, larger energy spread) with significant shot-to-shot variation in energy and pointing. High-quality optical pulses are therefore required for the production of stable, quasi-monoenergetic, self-injected electron beams, from underdense helium targets. The results reported in this paper were all obtained using an optimized, optically perfect laser pulse.

We proceed with the detailed study of the dependence of electron beam characteristics on plasma conditions and laser power. The laser pulse is focused close to the front edge of the nozzle. At high plasma density, $n_{e0} > 2 \times 10^{19}\mathrm{cm}^{-3}$, the electron beam spectrum was largely polychromatic with no quasi-monoenergetic features. A typical spectrum for the high-density case is depicted in Fig. 2(a). There is significant variation in the electron beam for different shots in terms of the energy spectrum and pointing. Increasing the power to 30–40 TW does not result in production of quasi-monoenergetic electrons. Significantly better results are obtained when the plasma density is reduced. Examples of such beams are shown in Figs. 3(a) and 3(b). With 30 TW on target and $n_{e0} = 10^{19}\,\mathrm{cm}^{-3}$, a monoenergetic beam with

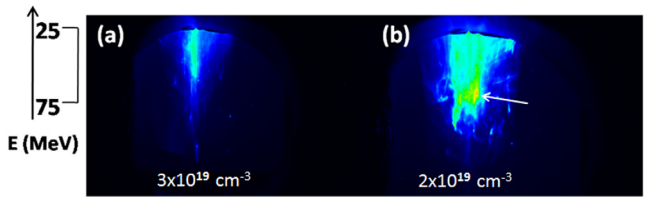

FIG. 2. Electron beams obtained from a laser-plasma accelerator in the low-power, high-density regime using underdense Helium target. (a) 20 TW, $n_{e0} = 3 \times 10^{19}\,\mathrm{cm}^{-3}$. (b) 20 TW, $n_{e0} = 2 \times 10^{19}\,\mathrm{cm}^{-3}$. In the former case, the electron beam is quasi-Maxwellian with no quasi-monoenergetic features. A monoenergetic feature (pointed at with an arrow) is observed in the lower density case (b); such features were observed in 10%–20% of shots with significant pointing and energy fluctuation. Raising the laser power beyond 30 TW does not help produce monoenergetic beams at these high densities.

central energy of ~100 MeV is observed. The beam has an angular divergence of ~8 mrad (measured along the non-dispersive axis) and a low energy tail that extends to 20 MeV (spectrometer cutoff). When the plasma density is further reduced to $8 \times 10^{18}\,\mathrm{cm}^{-3}$, the energy of the beam increases to 200 MeV, and the divergence decreases to 5 mrad. A prominent low-energy tail is still observed extending to the spectrometer cutoff at 20 MeV.

In order to optimize the beam quality, we performed a detailed study of the dependence of the electron beam characteristics on the plasma density. First, for a fixed plasma density, we varied the position of the focal plane of the laser pulse with respect to the front edge of the jet until the best quality beams were produced. Using an equivalent plane imaging system, we were able to control the position of the laser focus with respect to the jet with a precision of ± 0.5 mm. This imaging system also measured the pointing of the beam on target, $\pm 7\mu$ rad, which appears to be three orders of magnitude smaller than the pointing fluctuation of the electron beam. Once the optimal position of the focus was established, a feedback controlled valve was used to vary the backing pressure of helium on the jet. Interferometric measurements were used to determine that the plasma density is linear with the backing pressure. The plasma density on target was varied over a range from $2 \times 10^{18}\,\mathrm{cm}^{-3}$ to $4 \times 10^{19}\,\mathrm{cm}^{-3}$. The results obtained at higher densities are displayed in Figs. 2 and 3. Decrease of the density raises the beam energy until the highest energy electrons are produced at $n_{e0} = 5\text{–}6 \times 10^{18}\,\mathrm{cm}^{-3}$. Further reduction of density causes abrupt drop in energy, and eventually no beams are observed. The lowest density at which we could produce electron beams in our experiments is $4 \times 10^{18}\,\mathrm{cm}^{-3}$. We performed this optimization procedure for a variety of laser and plasma conditions. Representative results are shown in Fig. 4. Two different cases are considered: the results in Figs. 4(a) and 4(b) show that keeping the acceleration length fixed (3 mm jet) and using different laser powers, an optimal density can be found that produces a high-energy beam. As expected, higher laser power corresponds to higher electron energy. Indeed, the higher power means that the pulse self-focuses more rapidly, the bubble forms sooner, and electron gets self-injected earlier, having longer distance to accelerate. In addition, higher laser power means the larger bubble size, and, hence, larger fields acting on the self-injected electrons. Larger bubble size also means increase of the dephasing length.[28] Therefore, increasing plasma length in combination with higher laser power is favorable for boosting the electron energy. This is demonstrated using a 4 mm long jet. The electron distribution for this case is shown in Fig. 4(c). The highest energy beam obtained for 4 mm acceleration length has $E \approx 420$ MeV. This trend was found to hold at higher laser power and longer length scale jets as described later.

These results can be understood by making reference to the evolution of the laser pulse in the plasma. At the highest densities, the laser pulse is longer than a plasma period, $c\tau_L > \lambda_p$, and is strongly overcritical for relativistic self-focusing.[48–50] As a result, it experiences catastrophic self-focusing,[24] filamentation,[51] and longitudinal breakup.[52] As a result, several plasma buckets may be created, and electrons may be self-injected and accelerated in all of them,[21,52] producing broad energy distributions such as seen in Fig. 2. Reducing the plasma density slows down focusing of the pulse, reducing the risk of filamentation; once the pulse is shorter than a plasma period, it remains confined and self-guided within a single wake bucket—electron density bubble. In this case, electrons are injected and accelerated primarily within the single bubble. This process is scalable and tractable with reduced physics models.[24,26–28,33] Nonlinear optical

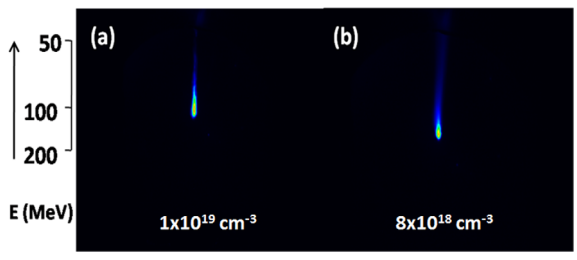

FIG. 3. Quasi-monoenergetic electron beams obtained with higher-power, lower-density plasma. (a) 30 TW, $n_{e0} = 10^{19}\,\mathrm{cm}^{-3}$. (b) 40 TW, $n_{e0} = 8 \times 10^{18}\,\mathrm{cm}^{-3}$. Reduction of plasma density leads to increase of the beam energy, and decrease in the energy spread and divergence.

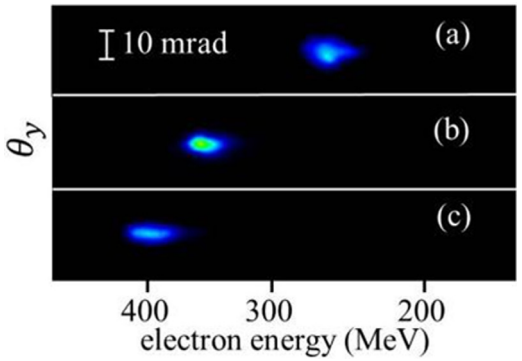

FIG. 4. Images of spectrally dispersed electron beams as a function of laser power and plasma density for two different acceleration lengths (a) $P = 34$ TW, $n_{e0} = 7.8 \times 10^{18}\,\mathrm{cm}^{-3}$; (b) $P = 42$ TW, $n_{e0} = 6 \times 10^{18}\,\mathrm{cm}^{-3}$; and (c) $P = 58$ TW, $n_{e0} = 5.3 \times 10^{18}\,\mathrm{cm}^{-3}$. Images (a) and (b) are obtained with a 3 mm jet. Image (c) is obtained with a 4 mm jet and a higher-resolution spectrometer. θ_x and θ_y denote the divergence angle in the horizontal and vertical direction.

evolution of the self-guided pulse may still cause deformations of the bubble, resulting in a continuous injection (the process also known as "dark current"), contaminating the electron spectra with poorly collimated, polychromatic background,[12–14,33] contributing to the generation of electron beams with significant lower energy tails, such as shown in Fig. 3. At even lower densities, injection of electrons into the bubble occurs over a limited length of the jet and the resulting electron beams have negligible low-energy tail (Fig. 4). Under these optimal conditions, the bubble forms before the end of the plasma, experiences minimal evolution, and creates a quasi-monoenergetic electron bunch.[29,33,54] Below a certain cutoff density, the bubble does not form during the laser transit through the plasma, and self-injection into the first bucket does not occur. For the experimental results depicted previously, this cutoff density corresponds to $4 \times 10^{18}\,\mathrm{cm}^{-3}$.

IV. PIC SIMULATIONS

To explain the origin of quasi-monoenergetic electron beams under conditions close to the optimal ones, we performed a series of 3D PIC simulations using a quasi-cylindrical, fully explicit electromagnetic PIC code calder-circ.[53] We present here the results for the regime close to that of Fig. 4(b). To suppress the sampling noise, 45 particles per cylindrical cell were taken, with the longitudinal resolution of 50 grid points per laser wavelength. To enable better comparison of the simulation with experimental data, electrons exiting the plasma were propagated through the experimental detection system using the particle tracking code GPT.

A Gaussian laser pulse, polarized in the x-direction, with 42 TW power, central wavelength $\lambda_0 = 0.805\,\mu\mathrm{m}$, and FWHM in intensity $\tau_L = 30$ fs, is focused into a spot size with the radius $r_0 = 13.6\,\mu\mathrm{m}$, and propagates in the positive z-direction. This waist size gives the Rayleigh length $z_R = (\pi/\lambda_0)r_0^2 \approx 0.72\,\mathrm{mm}$. The peak intensity in the focus is $1.77 \times 10^{19}\ \mathrm{W/cm}^{-2}$, corresponding to the normalized peak vector potential $a_0 = 2.53$. In the simulations, pre-ionized helium plasma with a trapezoidal profile extended from $z = 0$ to 3 mm (0.5 mm linear entrance and exit ramps, and a 2 mm plateau). Electron density in the plateau region, $n_{e0} = 7.2 \times 10^{18}\,\mathrm{cm}^{-2}$, corresponds to $\gamma_g = \omega_0/\omega_{pe} \approx 15.5$, $P/P_{\mathrm{cr}} \approx 10.8$ (where $P_{\mathrm{cr}} = 16.2\gamma_g^2$ GW is the critical power for relativistic self-focusing[48]), and $\omega_{pe}\tau_L = 4.54$.

The pulse is very overcritical, and its length makes a significant fraction of the electron Langmuir period. Therefore, once its focal plane is placed at the foot of the density ramp ($z = 0$), a very strong overfocusing occurs, and the bubble forms as soon as the pulse enters the density plateau. Due to flapping of the pulse tail inside the bubble, the bubble size oscillates, causing initiation and rapid termination of electron self-injection. Further on, the pulse front, constantly witnessing the nonlinear index down-ramp (viz. the front edge of the bubble), accumulates considerable red shift. Group velocity dispersion of the plasma slows down the red-shifted spectral components, leading to the front etching and self-compression of the pulse into a relativistically intense, few-cycle-length "piston."[55–57] As the pulse transforms into a piston, the bubble constantly elongates, trapping copious amounts of electrons, leading to the formation of poorly collimated bunch (charge and angular divergence an order of magnitude higher than observed in the experiment). This unfavorable dynamical scenario featuring massive continuous injection ("dark current"), leading to a catastrophic emittance dilution, was observed by various authors[4,13,14] and has been recently explained by Kalmykov *et al.*[33,35] In this situation, the only way to produce a highly collimated electron beam with low-charge is to terminate acceleration before the piston forms, by either limiting the plasma length,[29,33,54] or delaying the laser focusing in a finite-length plasma. To explore the latter option, we made serial PIC runs, varying the positions of the pulse focal plane with respect to the plasma edge. The beams with parameters close to experimental ones have been recovered with a focal plane offset $z = -1$ mm (or $-1.4z_R$). This offset is at the limit of experimental uncertainty. With this focusing geometry, it takes $\sim 2/3$ of the plasma length to refocus the diverging laser pulse, create the bubble, and inject electrons; once the bubble forms late, the pulse front steepening remains insignificant, and continuous injection does not occur.

The structure of the plasma wake at different stages of pulse evolution is shown in Fig. 5. The pulse arriving into plasma has the spot size 70% larger than the waist size, and is diverging. Therefore, it takes nearly two Rayleigh lengths, or half of the plasma length to refocus it and to create the bubble (cf. Fig. 5(b)). It takes another half-mm for the laser to start diffracting again, and for the bubble to expand; it is only at this point, as is seen in Fig. 5(c), electrons start getting injected. By the end of the plateau, the bubble expansion stabilizes, and injection almost ceases. The resulting bunch is clearly seen in Fig. 5(d). The pulse self-compression at this point is insignificant, and continuous injection remains at low level, keeping the bunch quasi-monoenergetic, producing weak low-energy tail in the energy spectrum shown in Fig. 6(b). The electron distribution (angle and energy) measured in the laboratory under slightly different laser and plasma condition, Fig. 6(a), agrees fairly well with the simulated energy spectrum depicted in Fig. 6(b). At the same time, simulations overestimate the beam divergence roughly by a factor 3.5.

In conclusion of this section, a few important points are to be made. First, in support of the observed experimental trend, calder-circ simulations with the same focusing geometry confirmed the absence of injection into the first bucket, and revealed sharp reduction of electron energy gain at densities below $5.5 \times 10^{18}\,\mathrm{cm}^{-3}$. Second, we see that electrons get injected at less than a millimeter distance from the end of the plateau. Given the cold wavebreaking electric field, $E_{WB} \approx 260$ MV/mm, where $E_{WB} \approx 0.96(n_{e0}[\mathrm{cm}^{-3}])^{1/2}$ V/cm, and knowing that the accelerating gradient inside the bubble actually exceeds the cold wavebreaking limit, we find the simulation result noncontradictory. Third, electrons in Fig. 5(d) are obviously far from dephasing. However, pursuing acceleration until dephasing in this high-density regime unavoidably brings about the dark current, solely because the too dense plasma reshapes the pulse into a piston too soon. Therefore, based on the results of simulation, it is possible that production of optimal beams in the laboratory

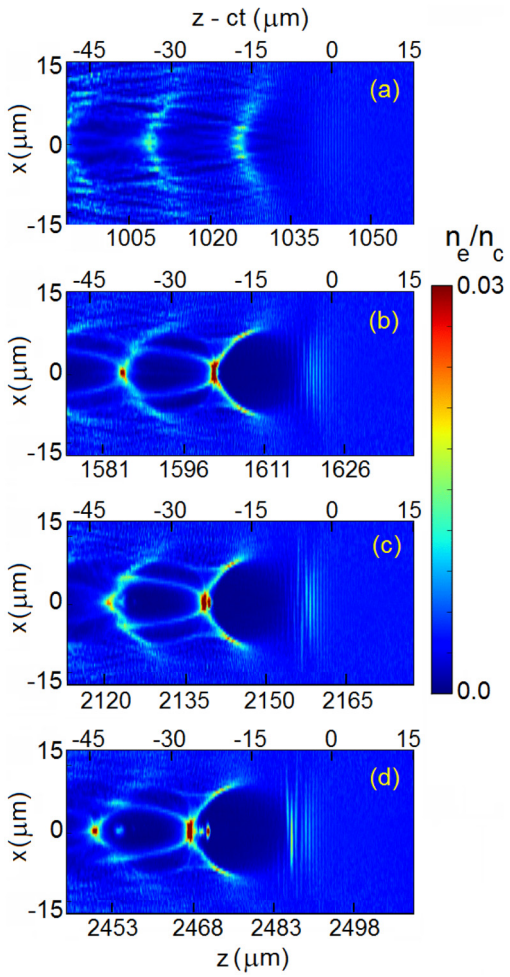

FIG. 5. Structure of the plasma wake at different stages of laser evolution (calder-circ simulation). Axis at the bottom of each panel shows the distance from the plasma border in microns; axis at the top of the panel shows the "co-moving" variable, z–it ct (also in microns; $z = ct$ is the trajectory of the pulse maximum in vacuum). Density cuts are taken in the plane of laser polarization. The pulse focal plane is situated at a distance $z = -1$ mm from the plasma border. Plasma extends from $z = 0$ to 3 mm. (a) 1 mm inside the plasma, the pulse is not yet focused, and the wake is still weakly nonlinear and unbroken; (b) 1.5 mm (or roughly $2z_R$) inside the plasma, the pulse eventually focuses and produces electron cavitation (the bubble); (c) the bubble starts expanding, initiating electron self-injection; (d) near the end of density plateau, the bubble stabilizes, self-injection terminates, and the quasi-monoenergetic beam forms.

was associated with the details of focusing geometry and transient dynamics of the laser pulse in plasma, rather than with the stable self-guiding of the pulse until electron dephasing and (or) pulse depletion.

V. HIGH ENERGY BEAMS FROM LONGER LENGTH JETS

In order to generate >500 MeV energy electron beams, the 70–90 TW laser pulse is focused onto a 5 or 10 mm supersonic jet from a slit nozzle. The experimental setup is similar to that shown in Fig. 1. The nozzles used in this case have a rectangular rather than a circular opening. This was necessary because the gas load associated with a cm-scale jet becomes significant both in terms of flow through the nozzle (viz. limitation on the load that can be handled by the solenoid valve) and the need for large pumps in order to remove the ambient gas in the chamber between successive laser shots. The jet profile measured interferometrically has a flat-top profile along the longitudinal direction and a Gaussian transverse profile. The absolute density calibration has been made using interferometric techniques. For a non-symmetric structure, two different axes are chosen to measure the interferometric fringe shift and a semi-analytic model is used to obtain the effective neutral density. The laser pulse self-channels through the medium and stays self-focused over the entire length of the jet. This self-channeling of the laser pulse is shown in Figs. 7(a) for a 5 mm jet and 7(b) for a 10 mm jet. The laser power in the former case is 80 TW, while in the latter case 90 TW. Given $z_R \approx 0.72$ mm, this demonstrates propagation of a 90 TW laser pulse over ~14 Rayleigh lengths, viz. over 10-mm distance without any external guiding (e.g., a pre-ionized capillary). Even though the power needed to maintain self-guiding over this large distance is rather high, the entire setup is simpler and more robust than devices based on guiding structures.

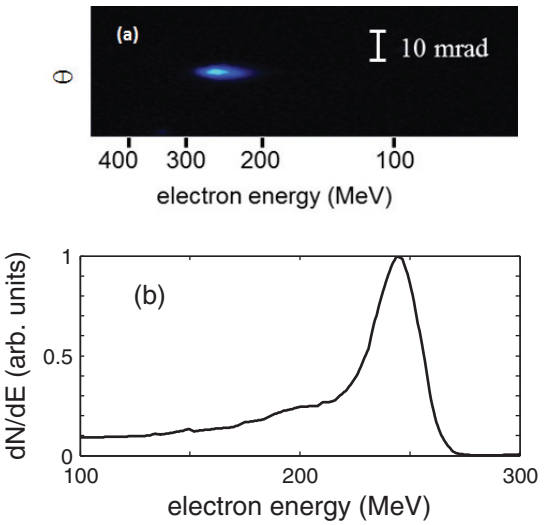

FIG. 6. Quasi-monoenergetic spectrum of electrons reaching the detector. Parameters of laboratory experiment correspond to 34 TW on target and the plasma density was 6×10^{18} cm^{-3}. For these conditions, the measured electron energy, $E \approx 250$ MeV (panel (a)), is in excellent agreement with the electron energy computed in the simulation of Fig. 5, $E \approx 240$ MeV. In the simulation, electron beam exiting the plasma was propagated through a detector identical to that used in experiment using the GPT code. Resulting computed spectrum (axial lineout of the detector image) is presented in the panel (b).

Under conditions when a high-energy laser pulse is incident on a 5 or 10 mm jet, a low-divergence, quasi-monoenergetic electron beam is produced. The higher laser

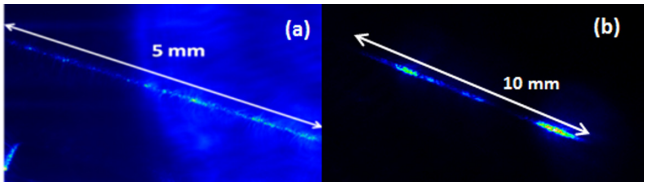

FIG. 7. Self-channeling of laser pulse through the plasma monitored by imaging the Thomson scattered light at 800 nm from the target. (a) 80 TW, $n_{e0} = 6 \times 10^{18}$ cm^{-3}. (b) 90 TW, $n_{e0} = 5 \times 10^{18}$ cm^{-3}. Based on an estimated Rayleigh range of 720 μm, (a) corresponds to propagation of the laser pulse over 7 Rayleigh ranges, while (b) corresponds to 14 Rayleigh ranges.

power combined with the longer acceleration length results in electron beams with significantly higher energy than that obtained for lower power and jets 3–4 mm length. As described previously for the supersonic jets, we performed a detailed study of the electron beam characteristics when high-power laser pulses interact with such long length plasma. To this end, we performed a parametric study for different acceleration lengths, laser power, and plasma density. The spectrometer used was modified by the use of a larger magnet with a stronger magnetic field in order to have the necessary resolution to perform accurate measurements of the electron beams with the energy above 500 MeV. Several single-shot measurements were performed with meter scale propagation of the electron beam in order to obtain precise measurement of the energy spread. We also studied the influence of the focal position of the laser with respect to the jet. Two specific cases were considered: (a) with the focus placed close the edge of the jet, similar to the studies for the 3 and 4 mm cylindrical nozzles and (b) with the focus located 1.5 mm relative inside the jet relative to position in (a). A detailed study was performed to study the characteristics of the electron beam produced from longer acceleration length slit nozzles.

For the 5 mm jet, high-energy beams could be obtained with the focus located inside the jet, at a 1.5 mm distance from the front edge. A sequence of shots is depicted in Fig. 8 for laser power 90 TW and $n_{e0} = 8 \times 10^{18}\,\mathrm{cm}^{-3}$. The quasi-monoenergetic beams have large energy spread and high charge (>50 pC). The pointing stability is ~10 mrad, significantly worse than that obtained for the 3–4 mm jets. Therefore, the use of high laser power, combined with high plasma density and long acceleration length leads to high-energy electrons. However, in this regime, the laser pulse is significantly modulated and continuous injection can occur over an extended length of the jet (see, e.g., the discussion of similar regime by Kneip *et al.*[13]). The strong nonlinear evolution of the system leads to strong fluctuation in the electron beam characteristics. Observation of the laser propagation via imaging of the scattered light from the plasma supports this thesis—the plasma channel fluctuates shot-to-shot both in terms of brightness and the length over which light emission is observed.

In order to produce high-energy beams in a more stable way, and reduce their energy spread, 80 TW pulses were focused onto the 5 mm jets using the same focusing configurations as above. The results for this case are shown in Fig. 9. In this case, the beam charge is lower than that depicted in Fig. 8. However, the beams are more monoenergetic with improved shot-to-shot pointing. For the case where the laser focus is placed inside the jet, quasi-monoenergetic beams with energy ~500 MeV are produced at a density of $6 \times 10^{19}\,\mathrm{cm}^{-3}$ as shown in Fig. 9(a). Below this density, no electron beams were observed in our experiments. With the laser focus placed closer to the edge of the nozzle, higher-energy electron beams could be produced at lower density. This is shown in Fig. 9(b) for a plasma density of $5 \times 10^{19}\,\mathrm{cm}^{-3}$. The beam energy did not increase further when higher power laser pulse was used.

In order to increase the beam energy even further we used a 10 mm long jet. The configuration is similar to that used for 5 mm jet. The laser power was 90 TW with the focus placed close to the front edge of the nozzle. The electron spectrum with a plasma density of $3.8 \times 10^{19}\,\mathrm{cm}^{-3}$ is shown in Fig. 10(a). For this case, we observe electron beams with the highest energies close to 800 MeV. In this low-density, high-power configuration, the electron beams are stable with

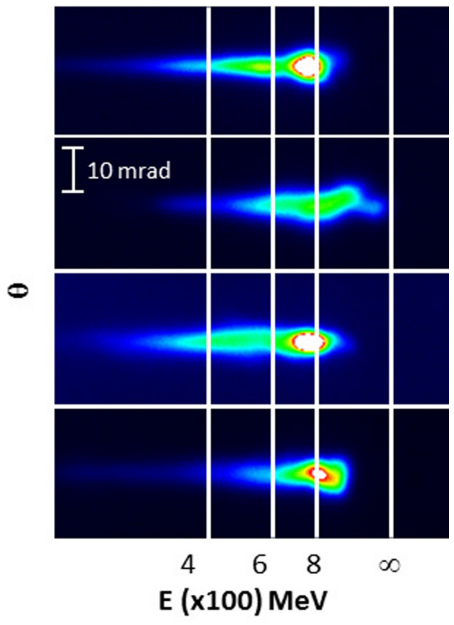

FIG. 8. Spectrum of electrons obtained with 5 mm slit jet. The laser pulse was at 90 TW and the focus was located inside plasma, at 1.5 mm distance from the edge of the nozzle. On average, the divergence of presented electron beams is ~10 mrad. The beam charge is rather high, 50–100 pC, but the energy spread and shot-to-shot fluctuations are significant as well. The mean energy is 710 ± 140 MeV, and the uncertainty in energy is primarily from the fluctuation in the beam pointing.

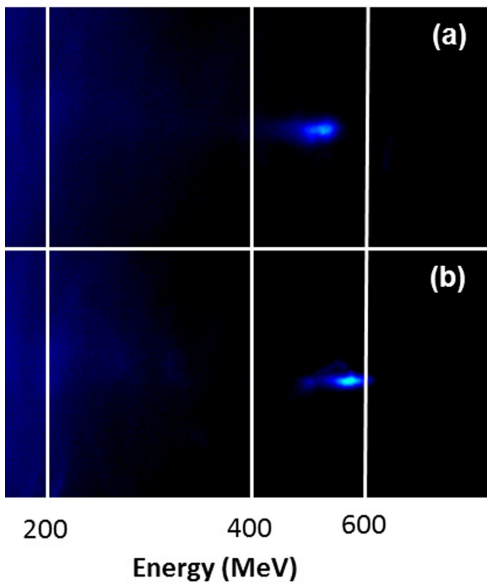

FIG. 9. Spectrum of electron beam obtained with 80 TW laser power and 5 mm slit nozzle for (a) 6×10^{18} (b) 5×10^{18}. The laser is focused 1.5 mm inside the jet. 550 MeV electron beams result when the focus is moved to the front edge of the nozzle and the plasma density is reduced to $5 \times 10^{19}\,\mathrm{cm}^{-3}$.

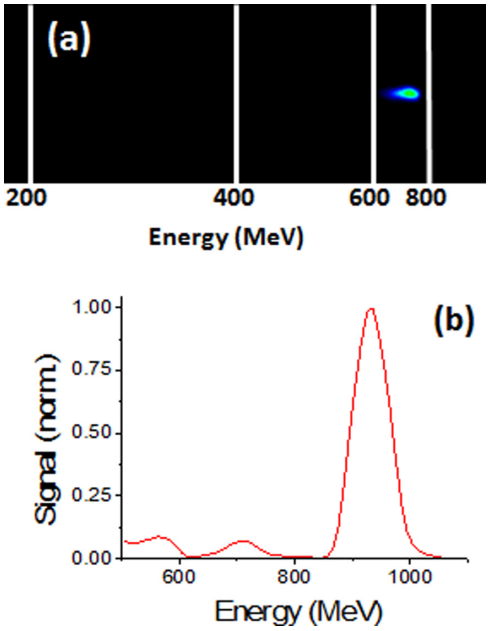

FIG. 10. (a) Spectrum of electron beam obtained with 90 TW laser power and 10 mm slit nozzle for plasma density 3.8×10^{18} and laser focused at the front of the nozzle. (b) Spectrum of electron beam obtained from CALDER-circ simulations with the same experimental geometry, plasma density 3.8×10^{18}, and 90 TW laser power on target. The measured energy is lower than the computed one on account of a non-ideal focus which results in a lowering of the effective laser power on target.

excellent shot-to-shot reproducibility. We supported these observations using calder-circ simulations. The computed spectrum for a plasma density of $3.25 \times 10^{19}\,\mathrm{cm}^{-3}$ and a laser power of 90 TW is shown in Fig. 10(b). The computed energy is higher than the experimentally measured value for two primary reasons: (a) the laser power on target is lower than the estimated 90 TW because of non-ideal focus and (b) the density used in the simulations is slightly lower than that used in the experiment. Despite these differences, the measurement and simulation agree well. We also verified that the threshold for self-injection matches that predicted by experiments.

VI. CONCLUSION

We have performed a detailed study of electron beam characteristics produced by high-energy, short-pulse lasers. The study encompasses optimization of beam characteristics as well as the generation of electron beams over a broad energy range. It is shown that by an appropriate choice of laser and plasma parameters and different acceleration lengths it is possible to produce stable electron beams over a broad energy range. A high-quality optical pulse is crucial for this work. In future, we propose to generate multi-GeV electron beams using PW level pulse made possible by the recent upgrade of the diocles laser system.

ACKNOWLEDGMENTS

This work was supported by the U.S. DOE Grant Nos. DE-FG02-05ER15663 and DE-FG02-08ER55000; DARPA Grant No. FA9550-09-1-0009; DTRA Grant No. HDTRA1-11-C-0001, and the U.S. DHS Grant No. 2007-DN-007-ER0007-02. Work of S.Y.K. and B.A.S. was supported in part by the NSF Grant No. PHY-1104683. The diocles laser is supported by the AFOSR under Contracts FA 9550-08-1-0232 and FA9550-07-1-0521. A.B. and E.L. were supported by LASERLAB-EUROPE/LAPTECH through EC FP7 Contract 228334. The authors thank CCRT (www-ccrt.cea.fr) for providing high-performance computing resources. We also thank Dr. Sicong Li of the University of Nebraska Medical Center for providing access to the 18 MeV accelerator.

[1]S. P. D. Mangles, C. D. Murphy, Z. Najmudin, A. G. R. Thomas, J. L. Collier, A. E. Dangor, E. J. Divall, P. S. Foster, J. G. Gallacher, C. J. Hooker, D. A. Jaroszynski, A. J. Langley, W. B. Mori, P. A. Norreys, F. S. Tsung, R. Viskup, B. R. Walton, and K. Krushelnick, Nature (London) **431**, 535 (2004).
[2]C. G. D. Geddes, Cs. Tóth, J. van Tilborg, E. Esarey, C. B. Schroeder, D. Bruhwiler, C. Nieter, J. Cary, and W. P. Leemans, Nature (London) **431**, 538 (2004).
[3]J. Faure, Y. Glinec, A. Pukhov, S. Kiselev, S. Gordienko, E. Lefebvre, J.-P. Rousseau, F. Burgy, and V. Malka, Nature (London) **431**, 541 (2004).
[4]V. Malka, J. Faure, Y. Glinec, A. Pukhov, and J.-P. Rousseau, Phys. Plasmas **12**, 056702 (2005).
[5]S. P. D. Mangles, A. G. R. Thomas, O. Lundh, F. Lindau, M. C. Kaluza, A. Persson, C.-G. Wahlström, K. Krushelnick, and Z. Najmudin, Phys. Plasmas **14**, 056702 (2007).
[6]J. Osterhoff, J. Osterhoff, A. Popp, Zs. Major, B. Marx, T. P. Rowlands-Rees, M. Fuchs, M. Geissler, R. Hörlein, B. Hidding, S. Becker, E. A. Peralta, U. Schramm, F. Grüner, D. Habs, F. Krausz, S. M. Hooker, and S. Karsch, Phys. Rev. Lett. **101**, 085002 (2008).
[7]A. Maksimchuk, N. Naumova, V. Chvykov, B. Hou, G. Kalintchenko, T. Matsuoka, J. Nees, P. Rousseau, G. Mourou, and V. Yanovsky, Appl. Phys. B: Lasers Opt. **89**, 201 (2007).
[8]K. Schmid, L. Veisz, F. Tavella, S. Benavides, R. Tautz, D. Herrmann, A. Buck, B. Hidding, A. Marcinkevicius, U. Schramm, M. Geissler, J. Meyer-ter-Vehn, D. Habs, and F. Krausz, Phys. Rev. Lett. **102**, 124801 (2009).
[9]S. M. Wiggins, R. C. Issac, G. H. Welsh, E. Brunetti, R. P. Shanks, M. P. Anania, S. Cipiccia, G. G. Manahan, C. Aniculaesei, B. Ersfeld, M. R. Islam, R. T. L. Burgess, G. Vieux, W. A. Gillespie, A. M. MacLeod, S. B. van der Geer, M. J. de Loos, and D. A. Jaroszynski, Plasma Phys. Controlled Fusion **52**, 124032 (2010).
[10]A. J. Gonsalves, K. Nakamura, C. Lin, D. Panasenko, S. Shiraishi, T. Sokollik, C. Benedetti, C. B. Schroeder, C. G. R. Geddes, J. van Tilborg, J. Osterhoff, E. Esarey, Cs. Tóth, and W. P. Leemans, Nat. Phys. **7**, 862 (2011).
[11]W. P. Leemans, B. Nagler, A. J. Gonsalves, Cs. Tóth, K. Nakamura, C. G. R. Geddes, E. Esarey, C. B. Schroeder, and S. M. Hooker, Nat. Phys. **2**, 696 (2006).
[12]N. A. M. Hafz, T. M. Jeong, I. Choi, S. K. Lee, K. H. Pae, V. V. Kulagin, J. H. Sung, T. J. Yu, K.-H. Hong, T. Hosokai, J. R. Cary, D.-K. Ko, and J. Lee, Nat. Photonics **2**, 571 (2008).
[13]S. Kneip, S. R. Nagel, S. F. Martins, S. P. D. Mangles, C. Bellei, O. Chekhlov, R. J. Clarke, N. Delerue, E. J. Divall, G. Doucas, K. Ertel, F. Fiúza, R. Fonseca, P. Foster, S. J. Hawkes, C. J. Hooker, K. Krushelnick, W. B. Mori, C. A. J. Palmer, K. Ta Phuoc, P. P. Rajeev, J. Schreiber, M. J. V. Streeter, D. Urner, J. Vieira, L. O. Silva, and Z. Najmudin, Phys. Rev. Lett. **103**, 035002 (2009).
[14]D. H. Froula, C. E. Clayton, T. Döppner, K. A. Marsh, C. P. J. Barty, L. Divol, R. A. Fonseca, S. H. Glenzer, C. Joshi, W. Lu, S. F. Martins, P. Michel, W. B. Mori, J. P. Palastro, B. B. Pollock, A. Pak, J. E. Ralph, J. S. Ross, C. W. Siders, L. O. Silva, and T. Wang, Phys. Rev. Lett. **103**, 215006 (2009).
[15]C. E. Clayton, J. E. Ralph, F. Albert, R. A. Fonseca, S. H. Glenzer, C. Joshi, W. Lu, K. A. Marsh, S. F. Martins, W. B. Mori, A. Pak, F. S. Tsung, B. B. Pollock, J. S. Ross, L. O. Silva, and D. H. Froula, Phys. Rev. Lett. **105**, 105003 (2010).
[16]J. S. Liu, C. Q. Xia, W. T. Wang, H. Y. Lu, Ch. Wang, A. H. Deng, W. T. Li, H. Zhang, X. Y. Liang, Y. X. Leng, X. M. Lu, C. Wang, J. Z. Wang, K. Nakajima, R. X. Li, and Z. Z. Xu, Phys. Rev. Lett. **107**, 035001 (2011).

[17]B. B. Pollock *et al.*, Phys. Rev. Lett. **107**, 045001 (2011).
[18]H. Lu, M. Liu, W. Wang, C. Wang, J. Liu, A. Deng, J. Xu, C. Xia, W. Li, H. Zhang, X. Lu, C. Wang, J. Wang, X. Liang, Y. Leng, B. Shen, K. Nakajima, R. Li, and Z. Xu, Appl. Phys. Lett. **99**, 091502 (2011).
[19]P. Dong, S. A. Reed, S. A. Yi, S. Kalmykov, G. Shvets, M. C. Downer, N. H. Matlis, W. P. Leemans, C. McGuffey, S. S. Bulanov, V. Chvykov, G. Kalintchenko, K. Krushelnick, A. Maksimchuk, T. Matsuoka, A. G. R. Thomas, and V. Yanovsky, Phys. Rev. Lett. **104**, 134801 (2010).
[20]P. Dong, S. A. Reed, S. A. Yi, S. Kalmykov, Z. Y. Li, G. Shvets, N. H. Matlis, C. McGuffey, S. S. Bulanov, V. Chvykov, G. Kalintchenko, K. Krushelnick, A. Maksimchuk, T. Matsuoka, A. G. R. Thomas, V. Yanovsky, and M. C. Downer, New J. Phys. **12**, 045016 (2010).
[21]M. H. Helle, D. Kaganovich, D. F. Gordon, and A. Ting, Phys. Rev. Lett. **105**, 105001 (2010).
[22]Z. Li, R. Zgadzaj, X. Wang, S. Reed, P. Dong, and M. C. Downer, Opt. Lett. **35**, 4087 (2010).
[23]J. B. Rosenzweig, B. Breizman, T. Katsouleas, and J. J. Su, Phys. Rev. A **44**, R6189 (1991).
[24]P. Mora and T. M. Antonsen, Jr., Phys. Rev. E **53**, R2068 (1996).
[25]A. Pukhov and J. Meyer-ter-Vehn, Appl. Phys. B: Lasers Opt. **74**, 355 (2002).
[26]S. Gordienko and A. Pukhov, Phys. Plasmas **12**, 043109 (2005).
[27]W. Lu, C. Huang, M. Zhou, M. Tzoufras, F. S. Tsung, W. B. Mori, and T. Katsouleas, Phys. Plasmas **13**, 056709 (2006).
[28]W. Lu, M. Tzoufras, C. Joshi, F. S. Tsung, W. B. Mori, J. Vieira, R. A. Fonseca, and L. O. Silva, Phys. Rev. ST Accel. Beams **10**, 061301 (2007).
[29]S. Kalmykov, S. A. Yi, V. Khudik, and G. Shvets, Phys. Rev. Lett. **103**, 135004 (2009).
[30]S. Y. Kalmykov, A. Beck, S. A. Yi, V. Khudik, B. A. Shadwick, E. Lefebvre, and M. C. Downer, AIP Conf. Proc. **1299**, 174 (2010).
[31]S. Y. Kalmykov, S. A. Yi, A. Beck, A. F. Lifschitz, X. Davoine, E. Lefebvre, A. Pukhov, V. Khudik, G. Shvets, S. A. Reed, P. Dong, X. Wang, D. Du, S. Bedacht, R. Zgadzaj, W. Henderson, A. Bernstein, G. Dyer, M. Martinez, E. Gaul, T. Ditmire, and M. C. Downer, New J. Phys. **12**, 045019 (2010).
[32]S. Y. Kalmykov, S. A. Yi, A. Beck, A. F. Lifschitz, X. Davoine, E. Lefebvre, V. Khudik, G. Shvets, and M. C. Downer, Plasma Phys. Controlled Fusion **53**, 014006 (2011).
[33]S. Y. Kalmykov, A. Beck, S. A., V. N. Khudik, M. C. Downer, E. Lefebvre, B. A. Shadwick, and D. P. Umstadter, Phys. Plasmas **18**, 056704 (2011).
[34]E. Esarey, C. B. Schroeder, and W. P. Leemans, Rev. Mod. Phys. **81**, 1229 (2009).
[35]S Y Kalmykov, A. Beck, X. Davoine, E. Lefebvre, and B. A. Shadwick, New J. Phys. **14**, 033025 (2012).
[36]S. Kneip, C. McGuffey, J. L. Martins, S. F. Martins, C. Bellei, V. Chvykov, F. Dollar, R. Fonseca, C. Huntington, G. Kalintchenko, A. Maksimchuk, S. P. D. Mangles, T. Matsuoka, S. R. Nagel, C. A. J. Palmer, J. Schreiber, K. Ta Phuoc, A. G. R. Thomas, V. Yanovsky, L. O. Silva, K. Krushelnick, and Z. Najmudin, Nat. Phys. **6**, 980 (2010).
[37]F. V. Hartemann, D. J. Gibson, W. J. Brown, A. Rousse, K. Ta Phuoc, V. Malka, J. Faure, and A. Pukhov, Phys. Rev. ST Accel. Beams **10**, 011301 (2007).
[38]P. Sprangle, B. Hafizi, and J. R. Peñano, Phys. Rev. ST Accel. Beams **12**, 050702 (2009).
[39]Y. Glinec, J. Faure, A. Guemnie-Tafo, V. Malka, H. Monard, J. P. Larbre, V. De Waele, J. L. Marignier, and M. Mostafavi, Rev. Sci. Instrum. **77**, 103301 (2006).
[40]See www.pulsar.nl/gpt for "General Particle Tracer (GPT), Pulsar Physics, Burghstraat 47, 5614 BC Eindhoven, The Netherlands".
[41]G. Pp̈lau, U. van Rienen, B. van der Geer, and M. de Loos, IEEE Trans. Magn. **40**, 714 (2004).
[42]S. B. van der Geer, O. J. Luiten, M. J. de Loos, G. Pöplau, and U. van Rienen, Inst. Phys. Conf. Ser. **175**, 101 (2005).
[43]V. Ramanathan, S. Banerjee, N. Powers, N. Cunningham, N. A. Chandler-Smith, K. Zhao, K. Brown, D. Umstadter, S. Clarke, S. Pozzi, J. Beene, C. R. Vane, and D. Schultz, Phys. Rev. ST Accel. Beams **13**, 104701 (2010).
[44]K. Schmid, A. Buck, C. M. S. Sears, J. M. Mikhailova, R. Tautz, D. Herrmann, M. Geissler, F. Krausz, and L. Veisz, Phys. Rev. ST Accel. Beams **13**, 091301 (2010).
[45]D. Umstadter, J. K. Kim, and E. Dodd, Phys. Rev. Lett. **76**, 2073 (1996).
[46]J. Faure, C. Rechatin, A. Norlin, A. Lifschitz, Y. Glinec, and V. Malka, Nature (London) **444**, 737 (2006).
[47]V. Malka, J. Faure, C. Rechatin, A. Ben-Ismaïl, J. K. Lim, X. Davoine, and E. Lefebvre, Phys. Plasmas **16**, 056703 (2009).
[48]G.-Z. Sun, E. Ott, Y. C. Lee, and P. Guzdar, Phys. Fluids **30**, 526 (1987).
[49]S. P. D. Mangles, A. G. R. Thomas, M. C. Kaluza, O. Lundh, F. Lindau, A. Persson, Z. Najmudin, C.-G. Wahlström, C. D. Murphy, C. Kamperidis, K. L. Lancaster, E. Divall, and K. Krushelnick, Plasma Phys. Controlled Fusion **48**, B83 (2006).
[50]M. Tzoufras, W. Lu, F. S. Tsung, C. Huang, W. B. Mori, T. Katsouleas, J. Vieira, R. A. Fonseca, and L. O. Silva, Phys. Plasmas **16**, 056705 (2009).
[51]A. G. R. Thomas, S. P. D. Mangles, C. D. Murphy, A. E. Dangor, P. S. Foster, J. G. Gallacher, D. A. Jaroszynski, C. Kamperidis, K. Krushelnick, K. L. Lancaster, P. A. Norreys, R. Viskup, and Z. Najmudin, Plasma Phys. Controlled Fusion **51**, 023010 (2009).
[52]B. Hidding, M. Geissler, G. Pretzler, K.-U. Amthor, H. Schwoerer, S. Karsch, L. Veisz, K. Schmid, and R. Sauerbrey, Phys. Plasmas **16**, 043105 (2009).
[53]A. F. Lifschitz, X. Davoine, E. Lefebvre, J. Faure, C. Rechatin, and V. Malka, J. Comput. Phys. **228**, 1803 (2009).
[54]N. A. M. Hafz, S. K. Lee, T. M. Jeong, and J. Lee, Nucl. Instrum. Methods Phys. Res. A **637**, S51 (2011).
[55]F. S. Tsung, C. Ren, L. O. Silva, W. B. Mori, and T. Katsouleas, Proc. Natl. Acad. Sci. U.S.A. **99**, 29 (2002).
[56]M. Lontano and I. G. Murusidze, Opt. Express **11**, 248 (2003).
[57]J. Faure, Y. Glinec, J. J. Santos, F. Ewald, J. P. Rousseau, S. Kiselev, A. Pukhov, T. Hosokai, and V. Malka, Phys. Rev. Lett. **95**, 205003 (2005).